Physica Scripta

PAPER

Quantum phase transitions in a Ξ-type atom-cavity QED system

Leilei Ping[1], **Yongfa Zhu**[2], **Shan Huang**[1] and **Lei Li**[1]

[1] School of Mathematics and Physics, Jingchu University of Technology, Jingmen 448000, People's Republic of China
[2] School of Chemistry and Chemical Engineering, Hubei Polytechnic University, Huangshi 435003, People's Republic of China

E-mail: huangshan0907@qq.com

Keywords: cavity QED, quantum phase transitions, three-level model, first-order quantum phase transition

OPEN ACCESS

RECEIVED
4 September 2024

REVISED
14 March 2025

ACCEPTED FOR PUBLICATION
12 May 2025

PUBLISHED
29 May 2025

Abstract

We theoretically investigated the influence of an atom's third energy level on quantum phase transitions in a Ξ-type atom-cavity quantum electrodynamics system driven by a coherent field. Through numerical simulations, we demonstrate that for a resonant two-level atom, the critical driving strength for quantum phase transitions scales linearly with the atom-cavity coupling strength. Analysis of the Wigner function confirms the occurrence of first-order quantum phase transitions, characterized by the emergence of coexistence states and symmetry breaking. Introducing a third atomic energy level under resonant conditions inhibits such phase transitions; however, detuning this level under specific parameters promotes them. By modulating the detuning of the third energy level, one can effectively control the critical conditions for quantum phase transitions in this system. These findings hold potential of applications in optically controlled phase transitions, precision measurements, and laser physics.

1. Introduction

Quantum phase transitions are driven by quantum fluctuations rather than thermal factors. When the absolute temperature of the system approaches zero, all thermal motion ceases, however, according to the Heisenberg uncertainty principle, the coordinates and momentum of microscopic particles cannot be simultaneously determined, meaning that particles still possess 'zero-point energy' and exhibit quantum fluctuations. These microscopic quantum fluctuations can drive the system from one phase to another, resulting in quantum phase transitions [1–4].

Since Dicke's pioneering work [5], collective superradiant phase transitions in large ensembles of atoms (or artificial atoms) have attracted significant attention and become a central focus of research in areas such as cavity quantum electrodynamics (QED) and circuit QED [3, 6–10]. Over the past few decades, research has predominantly centered around the two-level Dicke model and the Tavis-Cummings model [10–13]. As research has advanced, these models have been extended to three-level, multi-level, and more complex atomic systems [14–17]. Moreover, the focus of study has shifted from closed systems to open systems with driving and dissipation [10, 12, 18].

Research on quantum phase transitions in cavity QED systems has predominantly focused on many-particle systems within the thermodynamic limit. Nevertheless, exploring quantum phase transitions in single-particle systems holds great potential [19, 20]. Recent research has uncovered that quantum phase transitions can also occur in single-particle systems, thus broadening the scope of quantum phase transition research from many-particle to single-particle systems [21–24]. Compared to many-particle systems, single-particle systems eliminate interparticle interactions, making them easier to realize and control. Furthermore, single-particle systems can avoid methodological errors caused by over-approximation and thus pursue an exact solution [25–28].

Quantum phase transitions can be classified as first-order or second-order based on the nature of the transition, including changes in the system's quantum state and its critical behavior near the transition point [29, 30]. In a first-order quantum phase transition, the system's ground state undergoes a discontinuous change at the critical point, which may be accompanied by symmetry breaking or a drastic reconfiguration of the system's structure [30–34]. In contrast, second-order quantum phase transitions are characterized by a

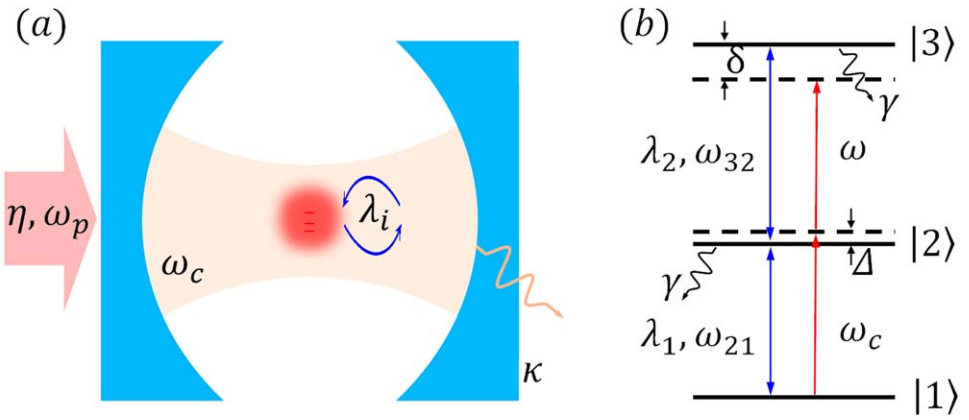

Figure 1. (a) Schematic of the system with a Ξ-typed three-level atom coupled to a single-mode cavity field driven by a coherent field with strength η and frequency ω_p. The loss rates of the cavity field and atom are κ and γ, respectively. (b) Level scheme of the atom indicating the parameters of the Hamiltonian in equation (1).

continuous but non-analytic evolution of the system's quantum state. Near the critical point, quantum fluctuations are significantly enhanced, leading to the divergence of certain physical observables, such as photon number fluctuations and correlation functions [35, 36]. A key feature of first-order quantum phase transitions is the coexistence of different phases or bistability. In many cases, first-order transitions exhibit a coexistence region, where multiple phases exist simultaneously. Therefore, the presence or absence of such coexisting phases within finite-size systems can be used as a criterion to distinguish first-order quantum phase transitions in quantum simulations.

Additionally, quantum phase transitions can be characterized using various methods, including the energy density functional, entanglement entropy and fidelity [37], photon-number distribution, Wigner function [38–40], and steady-state Q function [21, 41]. In quantum optics, the Wigner function is typically represented in phase space within the coherent state framework, where $\hat{X} = (\hat{a} + \hat{a}^\dagger)/2$ and $\hat{Y} = (\hat{a} - \hat{a}^\dagger)/2i$. These operators are dimensionless scaled position and momentum operators, respectively. Their coherent-state expectation values are $\langle \hat{X} \rangle = (\alpha + \alpha^*)/2 = \mathrm{Re}(\alpha)$ and $\langle \hat{Y} \rangle = (\alpha - \alpha^*)/2 = \mathrm{Im}(\alpha)$, so the complex α-plane serves as phase space, with the center of a coherent state located at $|\alpha| = \sqrt{\langle n \rangle}$ [39, 40]. In phase space, the vacuum state appears as a Gaussian distribution centered at the origin, with its spread characterizing quantum fluctuations. When displaced by a translation operator, it forms a coherent state, where the displacement from the origin approximately corresponds to the mean photon number in the cavity. The position of a coherent state in phase space can be associated with different phases in certain phase transition scenarios [42]. By analyzing the Wigner function's distribution in phase space, one can infer the quantum state of the photons inside the cavity [6, 43].

In this study, a system of Ξ-typed three-level atom interacting with a single-mode cavity is investigated [44], where the cavity field is driven by a coherent field. The influence of atomic energy levels on intracavity photons is studied, the phase transition of the system is analyzed from the perspective of the Wigner function in phase space [45], and a method for controlling the phase transition is proposed. The paper is organized as follows. Section 2 introduces the system model and presents its Hamiltonian. The numerical simulation results are discussed in Section 3. Finally, the conclusions are provided in section 4.

2. Model and Hamiltonian

We consider a Ξ-type three-level atom interacting with a single-mode cavity, with the cavity field subject to a coherent field drive [46]. As shown in figure 1(a), the atom-cavity coupling strengths are denoted by $\lambda_i (i = 1, 2)$, and the frequencies of the cavity field and driving field are ω_c and ω_p, respectively. In a frame rotating with frequency ω_p, the Hamiltonian of the system can be written as ($\hbar = 1$):

$$\begin{aligned} H = {} & \Delta_c\, a^\dagger a + \Delta\sigma_{22} + \delta\sigma_{33} \\ & + \lambda_1(a^\dagger\sigma_{12} + a\sigma_{21}) + \lambda_2(a^\dagger\sigma_{23} + a\sigma_{32}) \\ & + \eta(a + a^\dagger) \end{aligned} \tag{1}$$

where $a(a^\dagger)$ is the annihilation (creation) operator of the cavity mode, and $\sigma_{i,j} = |i\rangle\langle j| (i, j = 1, 2, 3)$ represent the atomic transition operators. Here, $\Delta_c = \omega_c - \omega_p$ is the detuning between the cavity field and the driving field, $\Delta = \omega_{21} - \omega_p$ and $\delta = \omega_{32} - \omega_p$ are the detunings of the atom relative to the driving field, ω_{ij} denotes the

transition frequency between level $|i\rangle$ and the level $|j\rangle$, as shown schematically in figure 1(b). The atom-cavity coupling strengths corresponding to the transitions $|1\rangle \leftrightarrow |2\rangle$ and $|2\rangle \leftrightarrow |3\rangle$ are λ_1 and λ_2, respectively.

The dynamic evolution of this three-level model system is described by the master equation for density matrix ρ [41]:

$$\frac{\partial}{\partial t}\rho = -i[H,\ \rho] + \mathcal{L}_\kappa(\rho) + \mathcal{L}_\gamma(\rho) \tag{2}$$

where $\mathcal{L}_\kappa(\rho) = \frac{\kappa}{2}(2a\rho a^\dagger - a^\dagger a\rho - \rho a^\dagger a)$ and $\mathcal{L}_\gamma(\rho) = \frac{\gamma_1}{2}(2\sigma_{21}\rho\sigma_{12} - \sigma_{12}\sigma_{21}\rho - \rho\sigma_{12}\sigma_{21}) + \frac{\gamma_2}{2}(2\sigma_{32}\rho\sigma_{23} - \sigma_{23}\sigma_{32}\rho - \rho\sigma_{23}\sigma_{32})$ are the dissipations of the cavity and atom, respectively [47].

For dissipative systems, we are interested in the steady-state atom-cavity dynamics occurring over timescales much longer than the cavity photon lifetime κ^{-1}. In this regime, the left-hand side of equation (2) can be set to zero to obtain the steady-state solution of the system [13]. However, due to the system's complexity and the non-integrability of the solutions, analytical expressions for the steady-state are available only in special cases. For instance, when the cavity is resonantly driven without the atom (i.e., $\Delta_c = 0$, $\lambda_1 = \lambda_2 = 0$), the mean photon number in the cavity varies with the driving intensity as $\langle a^\dagger a\rangle \approx 4\eta^2/\kappa^2$. In contrast, when an atom is present in the cavity under resonance or small detuning conditions, or when quantum fluctuations are significant, the mean-field approximation, commonly used in quantum phase transition studies, becomes inadequate. Therefore, the quantum optics software package QuTip is utilized to perform full quantum simulations based on equation (2) [48]. In these simulations, the decay rates are assumed to be $\gamma_1 = \gamma_2 = 0.1\kappa$, and these parameters remain constant throughout.

3. Results

To analyze the impact of different atomic energy levels on the system, we performed full quantum simulations to calculate the variations of the steady-state mean photon number in the cavity under different detunings, driving strengths, and atom-cavity coupling strengths. In our work, the atom has only three energy levels, so the reliability of the quantum simulation results primarily depends on the choice of the cavity photon Hilbert space. In theory, the largera photon space the better accuracy. However, increasing the photon space requires more computational resources and longer running times.

In figure 2(b), we present the simulation results for different photon spaces, empty cavity and a two-level atom inside the cavity. The black dotted line represents the analytical result given by $\langle a^\dagger a\rangle \approx 4\eta^2/\kappa^2$ for the resonantly driven empty cavity. When the driving strength $\eta/\kappa < 3$, all photon spaces can yield the same results. As the drive strength increases, however, the steady-state mean photon number in certain photon spaces exhibits a peak, after which it decreases and stabilizes. This behavior arises from the simulation process, where the photon exceeds the available photon space, leading to truncation errors. However, when an atom is added to the cavity, it reduces the mean photon number, thereby mitigating truncation errors. Taking all factors into account, in the subsequent simulations, we set the photon space $N_{ph} = 200$. This ensures that, for a two-level atom, results with photon below $\eta/\kappa < 8$ are reliable, while for a three-level atom, simulation results within $\eta/\kappa < 6$ are reliable, as shown in figure 3(b). Since our research primarily focuses on the impact of the third energy level on the quantum phase transition, it is sufficient to know that this region accommodates a large photon number distribution, the exact magnitude of the photon number layout, however, falls outside the scope of our study.

When the third energy level $|3\rangle$ is not considered, meaning that the atom in the cavity is only two-level atom (i.e., $\lambda_2 = 0$, $\delta = 0$) [49]. The variation of the steady-state mean photon number in the cavity with coupling strength λ_1/κ and driving strength η/κ is shown in figure 2(a). It is evident that there are two distinct regions: the upper left region (the red region within the white dashed line) indicates a high mean photon number in the cavity, represents the superradiant phase (macroscopic coherent state) where the atom is excited and the cavity hosts a large number of photons. In contrast, the lower right (blue) region represents the normal phase with a very sparse photon distribution. By examining the phase-space Wigner function shown in figure 2(c) and the probability distribution $P_i(i = 1, 2, 3)$ of the atom as shown in figure 3(a), it is clear that the cavity field in the vacuum state and the atom in the ground state. The region between these two phases is the critical region of the phase transition. Within this range, as the driving strength η/κ increases, the steady-state mean photon number in the cavity rises sharply.

The variation of the steady-state mean photon number with the driving strength η/κ for $\lambda_1/\kappa = 0$ (i.e., in the empty cavity) and $\lambda_1/\kappa = 10$ (i.e., a two-level atom in the cavity) is illustrated in figure 2(b). Although the two curves are nearly parallel, differing only in their thresholds as shown in the inset of figure 2(b), significant differences are observed in the phase space Wigner function distribution. The phase-space Wigner functions for the black, orange, blue, and red points in figure 2(b) are shown in figures 2(c)–(f), respectively. It can be seen that when there are no atoms in the cavity (i.e., the empty cavity case), as the driving strength increases, the phase-space Wigner function shifts away from the origin, indicating the transition of the cavity field from the vacuum

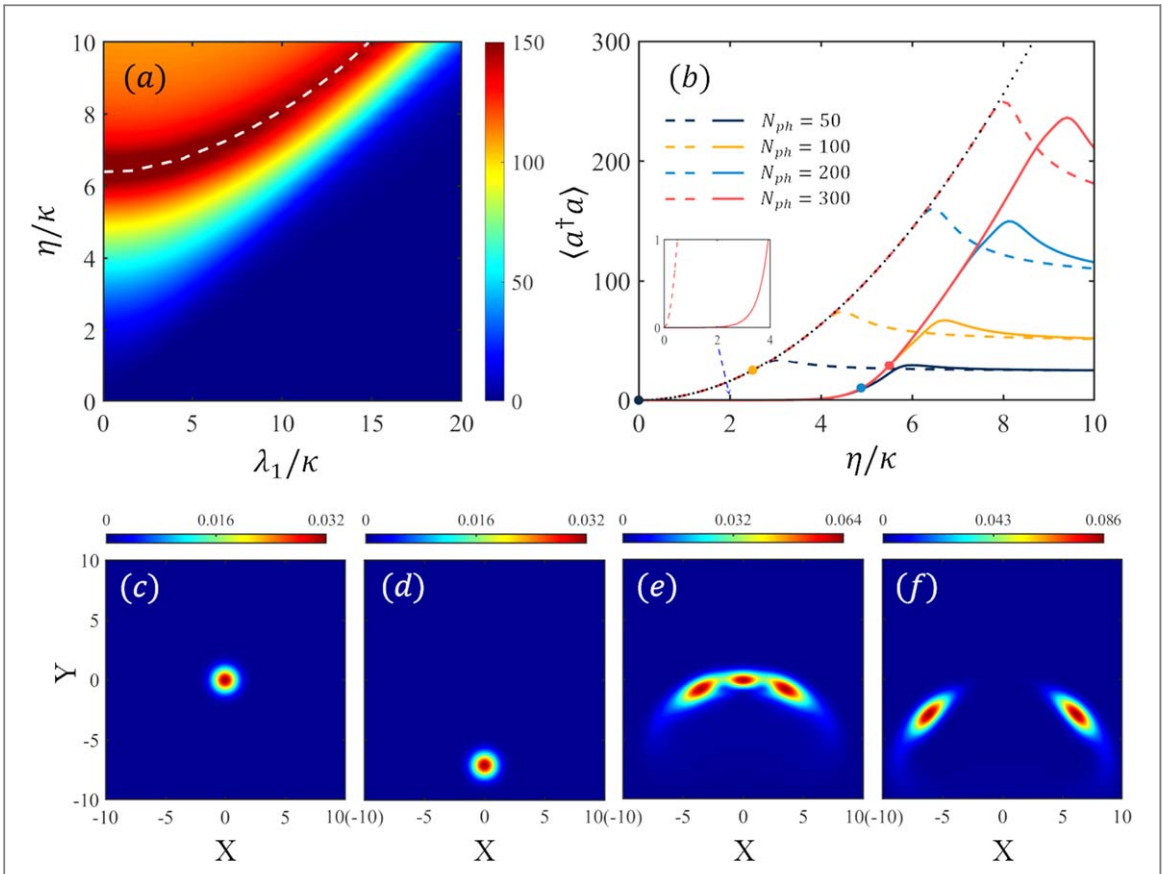

Figure 2. (a) The steady-state mean photon number $\langle a^\dagger a\rangle$ as a function of the coupling strength λ_1/κ and the driving strength η/κ. (b) The mean photon number $\langle a^\dagger a\rangle$ in the steady state varies with the driving strength η/κ for $\lambda_1/\kappa = 0$ (dashed line) and $\lambda_1/\kappa = 10$ (solid line), the dotted line in the figure represents the analytical expression $\langle a^\dagger a\rangle \approx 4\eta^2/\kappa^2$ for the steady-state mean photon number inside the cavity without atom. (c~f) The Wigner function distributions in phase space under different conditions. (c) The vacuum state, $\lambda_1/\kappa = 0, \eta/\kappa = 0$. (d) The coherent state, $\lambda_1/\kappa = 0, \eta/\kappa = 2.5$. (e) The coexistence state of vacuum state and coherent state, $\lambda_1/\kappa = 10, \eta/\kappa = 4.9$. (f) The coherent state with two phases, $\lambda_1/\kappa = 10, \eta/\kappa = 5.5$. Here, the other parameters are set to $\Delta_c = \Delta = \delta = 0, \lambda_2 = 0$.

state figure 2(c) to a coherent state figure 2(d). During this transition, the coherent state maintains a Gaussian distribution, and no symmetry breaking occurs.

However, when a two-level atom is present in the cavity($\lambda_1/\kappa = 10$), the Wigner function exhibits a characteristic evolution as the driving strength increases. Initially, the cavity field is in the vacuum state, as depicted in figure 2(c). As the driving strength increases, the Wigner function transitions to a coexistence state, where vacuum and coherent states coexist, as shown in figure 2(e). With further enhancement of the driving field, the system evolves into a bimodal phase-space distribution, comprising two coherent states with different phases, as shown in figure 2(f). Notably, if the driving strength continues to increase, the two Gaussian distributions in figure 2(f) move further away from the origin, indicating a larger intracavity photon number. During this quantum phase transition, the contribution of the vacuum state gradually diminishes, while coherent state components emerge symmetrically about the origin and eventually dominate the photon statistics. Once the driving strength exceeds a critical threshold, the vacuum component is completely displaced, and the system transitions into the superradiant phase, marking the completion of a first-order phase transition [13, 50, 51]. Moreover, the appearance of two distinct Gaussian lobes in phase space provides direct evidence of symmetry breaking in the system.

Therefore, when a two-level atom is present in the cavity, a first-order phase transition can be achieved by modulating the driving strength η/κ while keeping the atom-cavity coupling strength λ_1/κ constant. Moreover, a larger value of λ_1/κ results in a higher the phase transition threshold. In figure 2(b), the nearly parallel solid and dashed lines indicate that once an atom is introduced into the cavity, the drive field initially interacts with the atom, when the atom is excited into a superposition state $(|1\rangle + |2\rangle)/2$ (rather than being fully excited to the $|2\rangle$), the drive field then primarily interacts with the cavity. At this point, although the steady-state mean photon number is similar to the case of the driving cavity, the system undergoes symmetry breaking, and the cavity photons exhibit two distinct phases [42].

To investigate the role of the third energy level $|3\rangle$ in the system's phase transition, we fix $\lambda_1/\kappa = 10$ throughout this study. When the third energy level is introduced under full resonance conditions

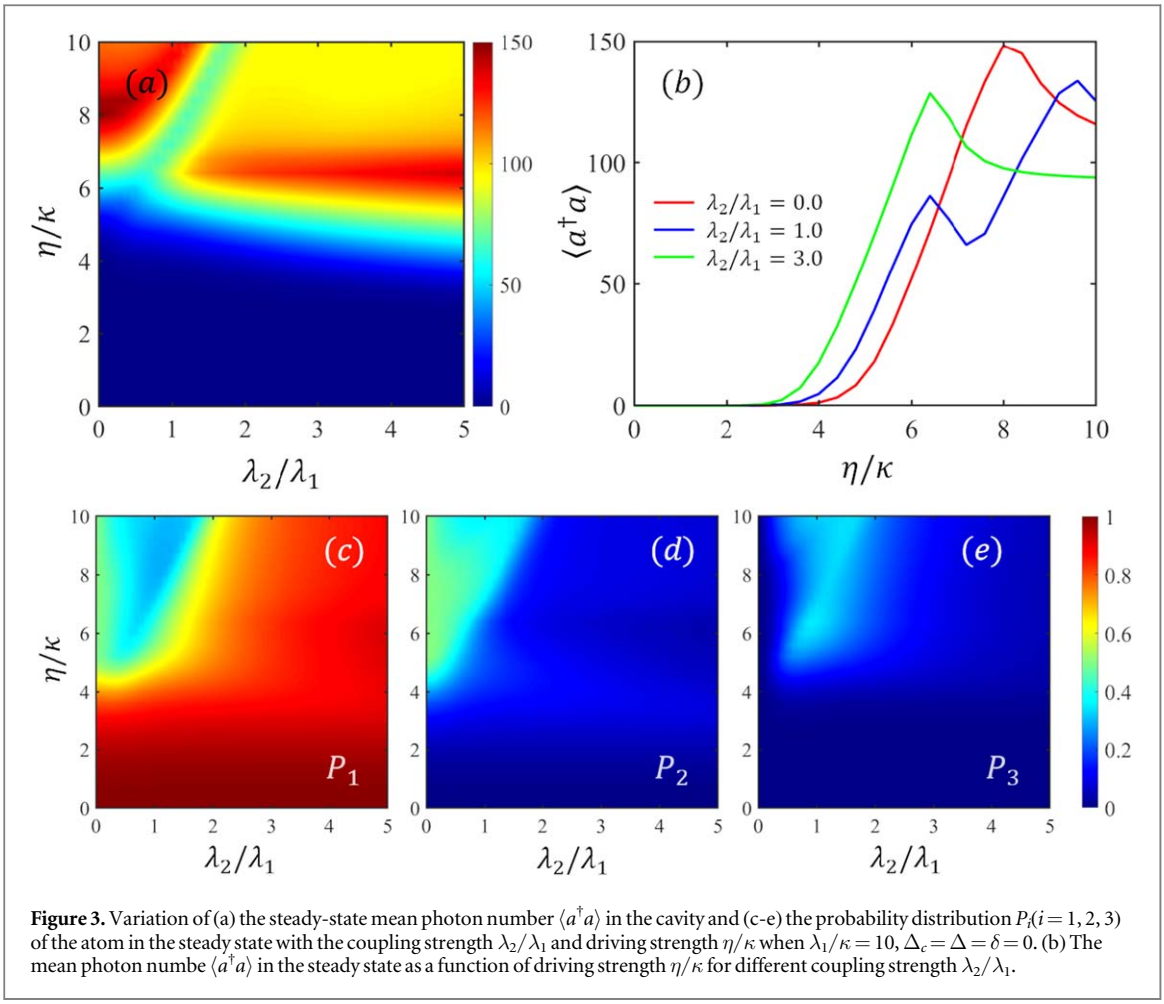

Figure 3. Variation of (a) the steady-state mean photon number $\langle a^\dagger a\rangle$ in the cavity and (c-e) the probability distribution $P_i(i=1,2,3)$ of the atom in the steady state with the coupling strength λ_2/λ_1 and driving strength η/κ when $\lambda_1/\kappa=10$, $\Delta_c=\Delta=\delta=0$. (b) The mean photon numbe $\langle a^\dagger a\rangle$ in the steady state as a function of driving strength η/κ for different coupling strength λ_2/λ_1.

($\Delta_c=\Delta=\delta=0$), figure 3(a) shows the steady-state mean photon number in the cavity as a function of λ_2/λ_1 and η/κ. For driving strengths $\eta/\kappa<2$, the cavity field remains in the vacuum state(i.e., the normal phase), regardless of the value of λ_2/λ_1. In the range $2<\eta/\kappa<6$, increasing λ_2/λ_1 leads to a rise of the mean photon number in the cavity. This suggests that enhancing the interaction between the $|2\rangle$ and $|3\rangle$ energy levels under the same driving strength promotes photon generation in the cavity. It remains to be verified whether these additional photons are generated through the atom-field interaction or via the interaction between the driving field and the cavity. When $\lambda_2/\lambda_1>2$ and $\eta/\kappa>6$, the cavity contains a large number of photons, the atom is no longer excited, and the system behaviors like a driven cavity.

To probe the deeper mechanisms, the probability distributions of the atomic states $P_i(i=1,2,3)$ under identical conditions are shown in figures 3(c)–(e). When $\eta/\kappa<2$, the excitation of the atom is insufficient due to the relatively low driving strength compared to the atom-cavity coupling strength λ_2/λ_1, leading to dominant occupation of the ground state $|1\rangle$. As η/κ increases, the atom begins to populate all three energy levels. However, when $\lambda_2/\lambda_1>3$, the $|2\rangle$ and $|3\rangle$ energy levels are no longer significantly excited, resulting in the atom predominantly residing in the ground state $|1\rangle$. In other words, under resonant conditions, when $\lambda_2/\lambda_1\ll 1$ and $\eta/\kappa<6$, the presence of the third energy level $|3\rangle$ can be regarded as a minor perturbation with negligible effect. Moreover, when $\lambda_2/\lambda_1<3$, as shown in figure 3(b), for $\eta/\kappa<6$, the emergence of $|3\rangle$ promotes the generation of cavity photons. In contrast, for $\lambda_2/\lambda_1>3$ the strong interaction between the $|2\rangle$ and $|3\rangle$ levels inhibits atomic excitation, thus hindering the occurrence of the first-order phase transition. At this point, the atom predominantly remains in the ground state $|1\rangle$, while the driving field primarily interacts with the cavity, leading to the generation of a substantial number of photons.

When the third energy level $|3\rangle$ is present and non-resonant ($\Delta_c=\Delta=0$ and $\delta/\kappa=10$), as illustrated in figure 4, both the steady-state mean photon number in the cavity and the probability P_3 for the atom to occupy state $|3\rangle$ exhibit significant differences. When the coupling strength $\lambda_2/\lambda_1<3$, photons emerge at the driving strength $\eta/\kappa<4$, lowering the critical threshold for phase transition. From the atomic perspective, this phenomenon occurs because the detuning increases the population of the third state $|3\rangle$. However, as λ_2/λ_1 increases, this effect diminishes, indicating that to effectively study the impact of detuning, the coupling strength should not be excessively large, and vice versa. When the driving strength is fixed at $\eta/\kappa=4$ and the coupling

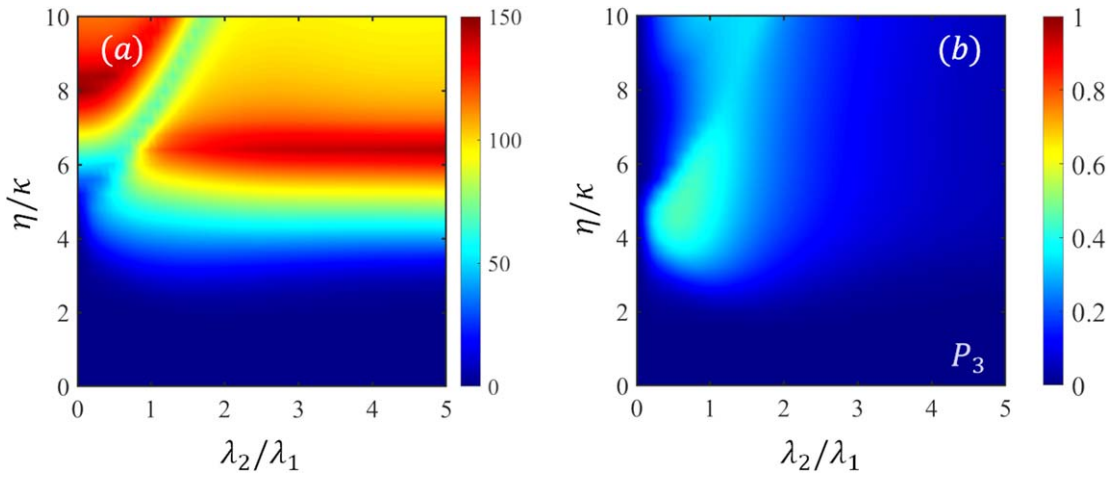

Figure 4. (a) The steady-state mean photon number $\langle a^\dagger a\rangle$ in the cavity and (b) the probability of the atom being in $|3\rangle$ in the steady state as a function of the coupling strength λ_2/λ_1 and driving strength η/κ, when $\lambda_1/\kappa = 10$, $\delta/\kappa = 10$ and $\Delta_c = \Delta = 0$.

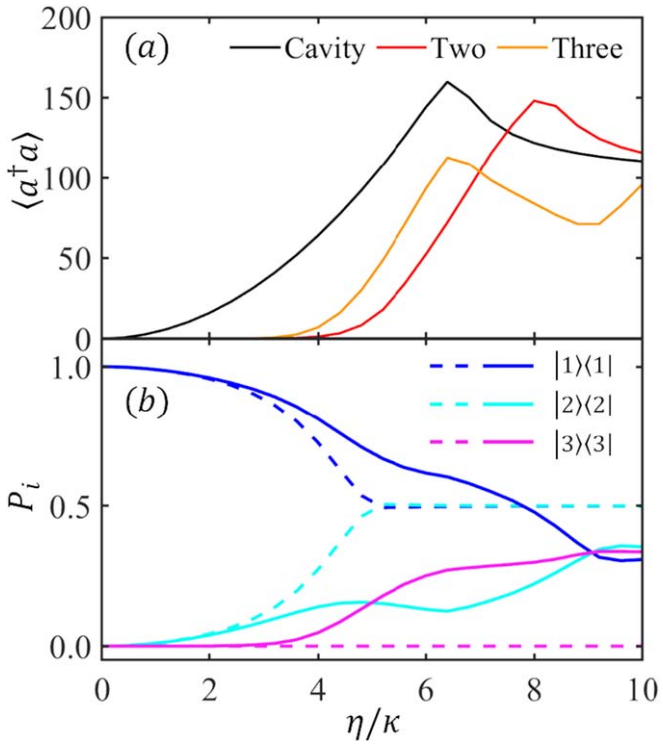

Figure 5. (a) The variation of the steady-state mean photon number $\langle a^\dagger a\rangle$ with the driving strength η/κ under three different scenarios: an empty cavity ($\lambda_2 = \lambda_1 = 0$), the cavity with two-level atom ($\lambda_1/\kappa = 10$, $\lambda_2/\lambda_1 = 0$) and the cavity with three-level atom ($\lambda_1/\kappa = 10$, $\lambda_2/\lambda_1 = 1.5$). (b) The probability distribution P_i of the atom in the steady state as a function of the driving strength η/κ as the atom within the cavity are two-level (dashed line) and three-level (solid line). Here, the other system parameters are set to $\Delta_c = \Delta = \delta = 0$.

strength $1 < \lambda_2/\lambda_1 < 3$, increasing both the detuning δ/κ and the coupling strength λ_2/λ_1 results in a significant increase in the number of cavity photons. The underlying mechanisms behind these two scenarios are different. Increasing λ_2/λ_1 weakens the atom-cavity interaction, causing the driving field to predominantly interact with the cavity. On the other hand, increasing the detuning δ/κ can increase the probability of P_3, within this range, photons primarily originate from the interaction between $|2\rangle$ and $|3\rangle$. Figure 4(b) corroborates this observation, showing that $|3\rangle$ is excited only when $\lambda_2/\lambda_1 < 3$. In this region, the interaction between $|2\rangle$ and $|3\rangle$ is significant, while in other regions the interaction between $|1\rangle$ and $|2\rangle$ is dominant.

In figure 5, we compare the steady-state mean photon number in the cavity and the probability distribution P_i for the atomic states as the drive strength η/κ increases for three scenarios: an empty cavity ($\lambda_1 = \lambda_2 = 0$), the cavity with a two-level atom ($\lambda_1/\kappa = 10$, $\lambda_2 = 0$), and the cavity with a three-level atom ($\lambda_1/\kappa = 10$,

$\lambda_2/\lambda_1 = 1.5$). The black line in figure 5(b) represents the empty cavity where photons are generated immediately upon the application of the drive field. The red line, corresponding to the two-level atom, shows a nearly parallel shift to the black line but with a higher threshold. Combined with the dashed line in figure 5(b), we find that as η/κ increases, the cavity photons initially interact with the atom. Once the atom is excited into a superposition state $(|1\rangle + |2\rangle)/2$, the system predominantly exhibits the characteristics of the driven cavity. The orange line, corresponding to the three-level atom, has a lower threshold than the two-level atom scenario but exhibits a higher steady-state mean photon number. This is because, under resonant driving, it is more difficult for the three-level atom to interact with the cavity field compared to the two-level atom. In the case of a two-level atom in the cavity, the driving field first excites the atom before affecting the cavity, while with a three-level atom this effect is less pronounced, meaning that photons are generated in the cavity only after the atom reaches a certain excitation level. Furthermore, figure 5(b) also highlights that when the driving strength $\eta/\kappa > 5$, a particle number inversion phenomenon occurs, which is a crucial observation with significant implications for laser physics.

4. Conclusion

In this work, we investigated the impact of the third energy level $|3\rangle$ of the atom on the quantum phase transition in a Ξ-type atom-cavity QED system, where the cavity field is driven by a coherent field. For a system containing a resonant two-level atom, the critical value of the quantum phase transition is directly proportional to the atom-cavity coupling strength; stronger coupling requires a higher driving field to induce the phase transition. Moreover, analysis of the Wigner function in phase space confirms that the system undergoes a first-order quantum phase transition. When a three-level atom is present, the inclusion of the third energy level suppresses the phase transition under resonant conditions. However, if the third level is detuned and specific conditions are met, it can facilitate the quantum phase transition. By manipulating the detuning of the third energy level, one can directly control the critical conditions for the quantum phase transition in this system. By comparing the variations of the steady-state mean photon number in the cavity and the probabilities of the atom being in different states under different conditions, we observed that with a two-level atom in the cavity, the driving field initially excites the atom before influencing the cavity. However, when the atom has three energy levels, this effect is diminished, although a population inversion phenomenon may still occur. In other words, cavity photons are generated only when the atom is excited under specific conditions. Furthermore, if the driving field is excessively strong, the atom's influence becomes negligible, and the system predominantly exhibits the interaction between the driving field and the cavity field. Our results have potential applications in optically controlled phase transitions, precision measurement, and laser physics.

Acknowledgments

This work was supported by the Natural Science Foundation of Hubei Province (No. 2023AFB429), the Scientific Research Program Key Project of Hubei Provincial Department of education (No.Q20234304), the Talent Introduction Project of Hubei Polytechnic University (No.21xjz01R) and the Scientific Research Projects of Jingchu University of Technology (Nos. ZD202308, ZD202317 and ZD202320).

Conflicts of interest

The authors declare no conflict of interest.

Data availability statement

All data that support the findings of this study are included within the article (and any supplementary files).

Authorship contribution statement

Leilei Ping: Model construction, Modifying original draft, Writing review & editing, Supervision. Yongfa Zhu: Theoretical derivation, Methodology, Numerical calculation, Writing original draft. Shan Huang: Theoretical derivation, Methodology, Numerical calculation. Lei Li: Writing- review & editing, Supervision, Data processing.

ORCID iDs

Yongfa Zhu https://orcid.org/0000-0002-8334-1577
Shan Huang https://orcid.org/0000-0003-4936-5775

References

[1] Hayn M and Brandes T 2017 *Phys. Rev. E* **95** 012153
[2] Sun L S, Zhao B, Yuan J-Q and Chen J 2021 *Opt. Express* **29** 7935
[3] Liu N, Li J and Liang J-Q 2013 *Phys. Rev. A* **87** 053623
[4] Xu Y and Pu H 2019 *Phys. Rev. Lett.* **122** 193201
[5] Dicke R H 1954 *Phys. Rev.* **93** 99
[6] Dombi A, Vukics A and Domokos P 2013 *J. Phys. B: At. Mol. Opt. Phys.* **46** 224010
[7] Liu N, Lian J, Ma J, Xiao L, Chen G, Liang J Q and Jia S 2011 *Phys. Rev. A* **83** 033601
[8] Zhao X, Liu N, Bai X and Liang J-Q 2017 *Ann. Phys.* **378** 448
[9] Baumann K, Guerlin C, Brennecke F and Esslinger T 2010 *Nature* **464** 1301
[10] Soriente M, Donner T, Chitra R and Zilberberg O 2018 *Phys. Rev. Lett.* **120** 183603
[11] Zou J H, Liu T, Feng M, Yang W L, Chen C Y and Twamley J 2013 *New J. Phys.* **15** 123032
[12] Adhikary K, Müstecaplıoğlu Ö. E. and Deb B 2023 *J. Phys. B: At. Mol. Opt.* **56** 135401
[13] Zhu C J, Ping L L, Yang Y P and Agarwal G S 2020 *Phys. Rev. Lett.* **124** 073602
[14] Nahmad-Achar E, Cordero S, Castaños O and López-Peña R 2014 *Phys. Scr.* **2014** 014033
[15] Nahmad-Achar E, Cordero S, López-Peña R and Castaños O 2014 *J. Phys. A: Math. Theor.* **47** 455301
[16] Cordero S, López-Peña R, Castaños O and Nahmad-Achar E 2013 *Phys. Rev. A* **87** 023805
[17] Baksic A, Nataf P and Ciuti C 2013 *Phys. Rev. A* **87** 023813
[18] Yu D and Genway S 2014 *Phys. Rev. A* **90** 043824
[19] Ashhab S 2013 *Phys. Rev. A* **87** 013826
[20] Larson J and Mavrogordatos T 2021 *The Jaynes-Cummings Model and its Descendants* (IOP Publishing) pp 2053–563
[21] Carmichael H J 2015 *Phys. Rev. X* **5** 031028
[22] Liu C and Huang J-F 2024 *Sci. China Phys. Mech. Astron.* **67** 210311
[23] Cai M-L, Liu Z-D, Zhao W-D, Wu Y-K, Mei Q-X, Jiang Y, He L, Zhang X, Zhou Z-C and Duan L-M 2021 *Nat. Commun.* **12** 1126
[24] Shen L-T, Tang C-Q, Shi Z, Wu H, Yang Z-B and Zheng S-B 2022 *Phys. Rev. A* **106** 023705
[25] Zhong P-G, Li C, Wang Y, Song J, Liu S-T, Jiang Y-Y and Xia Y 2019 *Phys. Rev. A* **99** 043829
[26] Gutiérrez-Jáuregui R and Agarwal G S 2021 *Phys. Rev. A* **103** 023714
[27] Chen Y-H, Qin W, Wang X, Miranowicz A and Nori F 2021 *Phys. Rev. Lett.* **126** 023602
[28] Ashhab S, Johansson J R, Zagoskin A M and Nori F 2007 *Phys. Rev. A* **75** 063414
[29] Vojta M 2003 *Rep. Prog. Phys.* **66** 2069
[30] Lee C F and Johnson N F 2004 *Phys. Rev. Lett.* **93** 083001
[31] Elsässer T, Nagorny B and Hemmerich A 2004 *Phys. Rev. A* **69** 033403
[32] Vengalattore M, Hafezi M, Lukin M D and Prentiss M 2008 *Phys. Rev. Lett.* **101** 063901
[33] Sedov D D, Kozin V K and Iorsh I V 2020 *Phys. Rev. Lett.* **125** 263606
[34] Hwang M-J, Rabl P and Plenio M B 2018 *Phys. Rev. A* **97** 013825
[35] Zheng R-H *et al* 2023 *Phys. Rev. Lett.* **131** 113601
[36] Feng M, Zhong Y, Liu T, Yan L, Yang W, Twamley J and Wang H 2015 *Nat. Commun.* **6** 7111
[37] Quezada L F and Nahmad-Achar E 2018 *Entropy* **20** 72
[38] Wigner E 1932 *Phys. Rev.* **40** 749
[39] Agarwal G S 2012 *Quantum Opt.* (Cambridge University Press)
[40] Gerry C C and Knight P L 2023 *Introductory Quantum Optics* (Cambridge University Press)
[41] Fink J M, Dombi A, Vukics A, Wallraff A and Domokos P 2017 *Phys. Rev. X* **7** 011012
[42] Kirton P and Keeling J 2017 *Phys. Rev. Lett.* **118** 123602
[43] Minganti F, Arkhipov I I, Miranowicz A and Nori F 2021 *New J. Phys.* **23** 122001
[44] Musa H T M O and Zhu Y 2022 *J. Mod. Opt.* **69** 475
[45] Leroux C, Govia L C G and Clerk A A 2017 *Phys. Rev. A* **96** 043834
[46] Skulte J, Kongkhambut P, Keßler H, Hemmerich A, Mathey L and Cosme J G 2021 *Phys. Rev. A* **104** 063705
[47] Li W, Zhu C J and Yang Y P 2021 *Opt. Express* **29** 42176
[48] Johansson J, Nation P and Nori F 2013 *Comput. Phys. Commun.* **184** 1234
[49] Gutiérrez-Jáuregui R and Carmichael H J 2018 *Phys. Rev. A* **98** 023804
[50] Luo X-Y, Zou Y-Q, Wu L-N, Liu Q, Han M-F, Tey M K and You L 2017 *Science* **355** 620
[51] Beaulieu G, Minganti F, Frasca S, Savona V, Felicetti S, Di Candia R and Scarlino P 2025 *Nat. Commun.* **16** 1954